Geophysical Research Letters

RESEARCH LETTER
10.1029/2022GL098923

Key Points:

- A quasi-continental survey through radar interferometry reveals present-day land subsidence hotspots in Central Mexico
- Subsidence correlates with hydraulic head changes and aquifer-systems' groundwater deficits, extractions and storage loss
- Semi-theoretical relationships enable assessment of compaction rates and volumes resulting from groundwater exploitation

Correspondence to:
F. Cigna,
f.cigna@isac.cnr.it

Citation:
Cigna, F., & Tapete, D. (2022). Land subsidence and aquifer-system storage loss in Central Mexico: A quasi-continental investigation with Sentinel-1 InSAR. *Geophysical Research Letters*, *4*, e2022GL098923. https://doi.org/10.1029/2022GL098923

Received 29 MAR 2022
Accepted 13 JUL 2022

Author Contributions:
Conceptualization: F. Cigna, D. Tapete
Data curation: F. Cigna, D. Tapete
Formal analysis: F. Cigna, D. Tapete
Investigation: F. Cigna, D. Tapete
Methodology: F. Cigna, D. Tapete
Project Administration: F. Cigna
Resources: F. Cigna, D. Tapete
Software: F. Cigna, D. Tapete
Validation: F. Cigna, D. Tapete
Visualization: F. Cigna, D. Tapete
Writing – original draft: F. Cigna, D. Tapete
Writing – review & editing: F. Cigna, D. Tapete

Land Subsidence and Aquifer-System Storage Loss in Central Mexico: A Quasi-Continental Investigation With Sentinel-1 InSAR

F. Cigna[1] **and D. Tapete**[2]

[1]National Research Council (CNR), Institute of Atmospheric Sciences and Climate (ISAC), Rome, Italy, [2]Italian Space Agency (ASI), Rome, Italy

Abstract Aquifers play an important role in addressing water needs worldwide. When overexploited, they may lose storage and compact, causing land subsidence and impacts on urban landscapes. Using Sentinel-1 satellite imagery, we perform the largest ever-made Interferometric Synthetic Aperture Radar (InSAR) survey over Mexico, across a 700,000 km^2 area hosting >85.2 million inhabitants. We estimate present-day subsidence rates for yet unmapped and well-known hotspots (e.g., −45 cm/year in Mexico City), and compute compaction volumes at >300 aquifer-systems (up to −60 hm^3/year at Mexico City Metropolitan Area). InSAR-derived aquifer-system compaction generally correlates well with groundwater deficits, extractions and storage changes from management reports. Semi-theoretical relationships for the whole Central Mexico and hydrological-administrative regions VII, VIII, and XIII, enable the assessment of compaction rates and volumes resulting from groundwater exploitation. These could be used to inform groundwater management strategies towards adaptation to climate change and future needs of a growing population.

Plain Language Summary Groundwater resources address a large component of water needs worldwide, especially in countries with extensive arid regions, such as Mexico. When aquifers are overexploited in excess of natural recharge, they may lose part of their storage capacity and compact, causing land subsidence. Impacts on urban landscapes, such as surface fracturing of buildings and transport networks, are very common in Central Mexico, where several aquifers are in deficit. In this work, we process satellite Sentinel-1 radar data with a multi-temporal interferometric method, to perform a quasi-continental survey of land deformation. The analysis enables the identification of several land subsidence hotspots (not only subsiding sites already known such as Mexico City, but also others previously unmapped), and the estimation of their present-day subsidence patterns and rates. Using satellite data, we compute compaction volumes of aquifer-systems and compare them with groundwater deficits, extractions and storage changes from official aquifer-system management reports. We found that satellite observations correlate well with aquifer-system data. We therefore derive some semi-theoretical relationships linking groundwater exploitation data with the resulting compaction. These relationships could be used to inform groundwater management strategies towards adaptation to climate change and future needs of a growing population.

1. Introduction

Aquifers host 30% of global freshwaters (Shiklomanov, 1993), and play an important role in addressing water needs worldwide, especially in countries with extensive arid regions (United Nations, 2022). In Mexico, 39.5% of the consumed water is supplied through ~35,300 hm^3/year groundwater, extracted from ~300,000 wells and used for agriculture (71%), public supply (21%), industry and electric energy (excluding hydroelectric) (8%) (CONAGUA, 2022b). Although Mexico is not considered "water-poor", large discrepancies in recharge and consumption rates and patterns exist: only 20% of the total annual rainfall occurs where 76% population lives and 90% irrigated lands are maintained (Hernandez, 2003). In 2020, the National Waters Commission (CONAGUA) identified 157 overexploited aquifers near densely populated cities and large farmlands, and 48 threatened by salinization and/or marine intrusion (CONAGUA, 2022b). Land subsidence resulting from groundwater overexploitation has also been documented in major cities of Central Mexico (Cabral-Cano et al., 2008; Carreon-Freyre et al., 2011). Topographic lowering, tilting and deformation, apparent uplifting of deeply founded structures, surface cracking and faulting are very common impacts that aquifer-system compaction causes on Mexican urban landscapes (Carreón Freyre, 2010; Figueroa-Miranda et al., 2018), and in many other countries (Galloway &

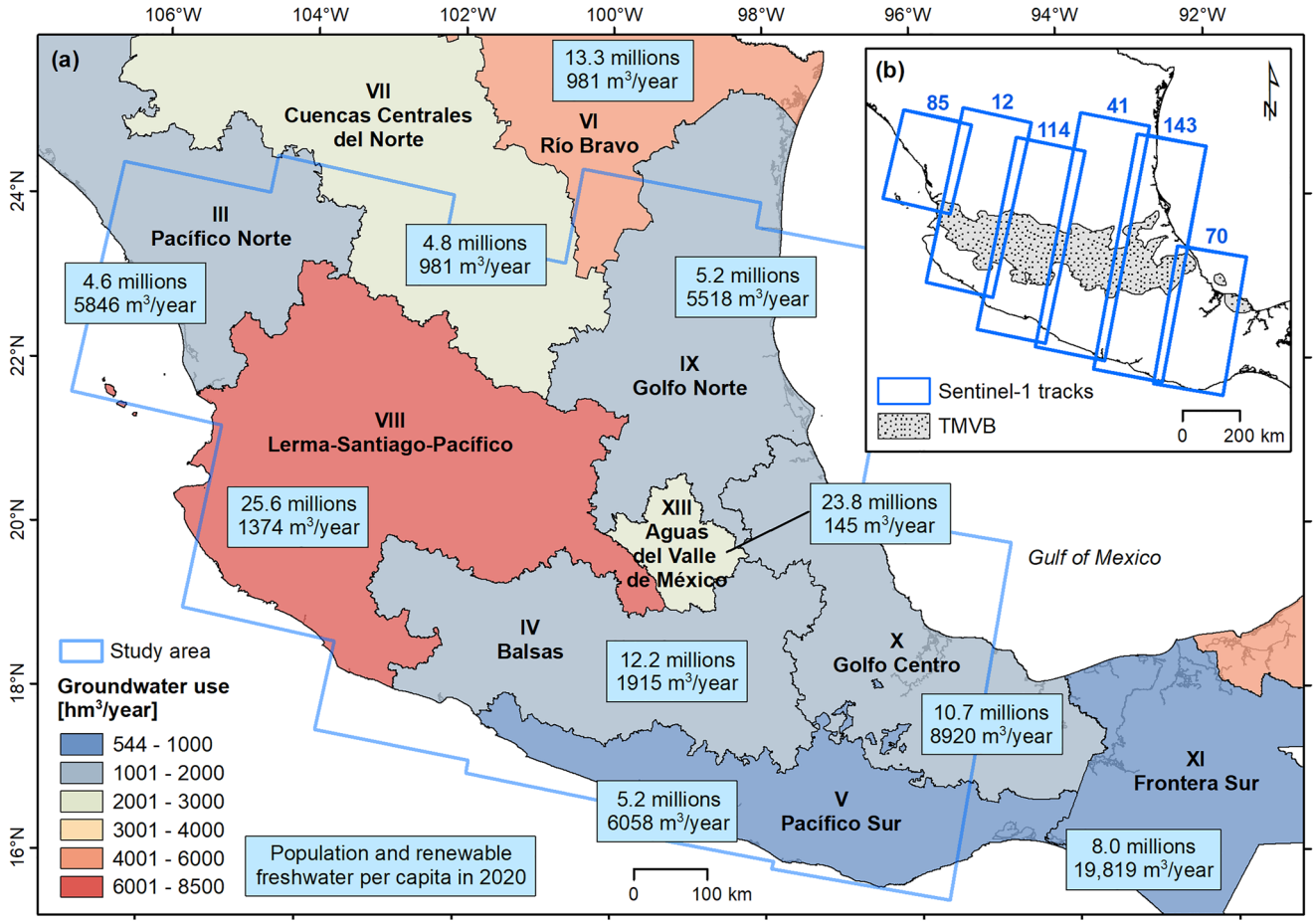

Figure 1. Location of the study area in Central Mexico: (a) Population, renewable freshwater per capita and groundwater use in each hydrological-administrative region; and (b) footprints of the six Sentinel-1 tracks used for the Interferometric Synthetic Aperture Radar (InSAR) survey, overlapped onto extent of the Trans-Mexican Volcanic Belt (TMVB). Maps created with ESRI ArcMap.

Burbey, 2011). Knowledge of aquifer-systems' hydraulic and geological properties is therefore essential to understand their response to groundwater withdrawal, identify pathways to sustainable groundwater management, and mitigate impacts due to overexploitation.

In this work, we analyze the correlation between land deformation, groundwater deficits, extractions and aquifer storage changes in the whole of Central Mexico. We focus on a 700,000 km^2 area hosting >85.2 million inhabitants (i.e., ~68% of the Mexican population; INEGI, 2022), and encompassing the Trans-Mexican Volcanic Belt (TMVB; Ferrari et al., 2012) and several hydrological-administrative regions (RHA), including Lerma-Santiago-Pacífico, Balsas and Aguas del Valle del México (Figure 1a). Here, yearly availability of renewable freshwater (that can be sustainably exploited) ranges between ~140 and ~8,900 m^3/inhabitant (CONAGUA, 2022b). The area encloses large discharge zones of regional groundwater flow systems (Kachadourian-Marras et al., 2020), and groundwater footprints of its aquifers are 9.1 ± 2.6 times their area (Gleeson et al., 2012). Licensed extractions amount to ~17,500 hm^3/year in total (CONAGUA, 2022b), and regional depletion rates reach 0.1 m/year (Wada et al., 2010).

We undertake a quasi-continental land subsidence hotspot survey through satellite Interferometric Synthetic Aperture Radar (InSAR; Rosen et al., 2000). Hydrogeological studies have started to use this technique along with piezometric data to estimate elastic and inelastic storage of aquifers worldwide (e.g., Bell et al., 2008; Bonì et al., 2016; Chaussard, Bürgmann, et al., 2014; Hoffmann et al., 2001; Miller et al., 2017; Ojha et al., 2018). While some wide-area (Chaussard, Wdowinski, et al., 2014; Cigna et al., 2019), multi-city (Castellazzi, Arroyo-Domínguez, et al., 2016) or single-city (e.g., Brunori et al., 2015; Cigna et al., 2012; Osmanoğlu

et al., 2011; Pacheco-Martínez et al., 2015) InSAR assessments exist for Central Mexico, an up-to-date snapshot of present-day subsidence has not yet been provided for this vast region as a whole. Moreover, none of such studies has investigated holistically how subsidence correlates with aquifer management data or piezometric records from the national monitoring network.

By filling these gaps, for the first time, we establish semi-theoretical relationships to assess the compaction rates and volumes resulting from groundwater exploitation, which could be used to inform future management strategies of this vital resource in Mexico and potentially other countries, toward adaptation to climate change impacts on the water balance, and changing needs and shifts in groundwater use by a growing world population.

2. Methods

2.1. Quasi-Continental InSAR Survey

We exploited 1677 C-band VV-polarized Interferometric Wide (IW) swath SAR scenes acquired by the Copernicus Sentinel-1 mission (Torres et al., 2012), along six descending tracks (Figure 1b). Each stack consists of ∼60 scenes with 12 days revisit, 250 km swath, 5 (ground range) by 20 (azimuth) m resolution, and 31°–46° incidence angles (θ). A 2 years-long period (2019–2020) allowed trading-off the yearly release of aquifer management data (Section 2.2) for SAR stacks sufficiently long to provide robust outputs.

We used the parallelized Small BAseline Subset (SBAS) InSAR method (Casu et al., 2014), adapted for IW data (Manunta et al., 2019) and integrated in ESA's Geohazards Exploitation Platform (GEP). Geohazards investigations in a few Mexican cities (Cigna & Tapete, 2021a, 2021b, 2022) proved this technique capable to estimate displacement velocity with mm/year accuracy against geodetic data (Cigna et al., 2021), and thus suitable to attempt a quasi-continental survey.

Interferograms were 20 × 5 multi-looked to reduce phase noise, resulting in ∼90 m ground spacing. Topographic components were subtracted using the 30 m resolution Shuttle Radar Topography Mission elevation model (Farr et al., 2007). As horizontal displacement components in the region are much lower than vertical (Blewitt et al., 2018), these were assumed negligible and SBAS-derived Line-of-Sight (LOS) estimates V_{LOS} were converted to the vertical direction as $V_U = V_{LOS}/\cos\theta$, with θ varying across the swath. The reference points were set within zones devoid of short-wavelength scale deformation (e.g., onto stable, non-consolidating lithologies), and outside well-known subsiding areas identified in past studies (Castellazzi et al., 2018; Chaussard, Wdowinski, et al., 2014; Cigna et al., 2019). No post-processing calibration between adjacent frames was done, to preserve the local reference of each dataset. This enabled filtering out regional signals (not of interest to study compaction at aquifer scale).

A continuous V_U map was generated via inverse distance weighting interpolation of point-wise outputs, and then spatially integrated (x,y) within each aquifer boundary. Assuming V_U indicates aquifer-system compaction, this enabled the computation of the compaction volume rate, ΔS_{sat}:

$$\Delta S_{sat} = \iint V_U(x, y)dx\,dy \quad (1)$$

2.2. Aquifer Balance and Storage

Groundwater balance parameters for 321 aquifer-systems were extracted from their latest management reports (CONAGUA, 2022a) and updates in the Official Federal Gazette (Secretaría de Gobernación, 2021a, 2021b). The balance refers to aquifer-systems considered as water-yielding hydraulic units (Poland et al., 1972), with their composing sediments and complex structure. Inputs into the system (i.e., recharge, R) include vertical recharge from rainfall/precipitation (P), horizontal inflow from adjacent aquifers (Q_{in}) and incidental recharge from irrigation, canal seepage and distribution and sewage network leaks (I). Outputs (i.e., discharge, D) are natural outflows, for example, evapo-transpiration (ET), horizontal outflow to other aquifers (Q_{out}), discharge through springs (Q_s) and baseflow to surface streams (Q_b), plus anthropogenic outflow through groundwater extraction (Q_{ext}). If $Q_{ext}/R \geq 1.1$, the system is "overexploited" (CONAGUA, 2022b).

The difference between recharge and natural and human-induced discharge in a given time period identifies the aquifer-system storage change (ΔS), either volumetric gain (if $\Delta S > 0$) or loss ($\Delta S < 0$):

$$\Delta S = R - D = P + Q_{\text{in}} + I - ET - Q_{\text{out}} - Q_s - Q_b - Q_{\text{ext}} \quad (2)$$

ΔS depends on hydraulic head change Δh and storativity (S^*) of the n layers i composing the system (i.e., the amount of water released from storage per unit aquifer surface A and Δh; derived from pumping tests, laboratory experiments, or lithology), and can be expressed based on the aquifer-system thickness change Δb:

$$\Delta S = \sum_{i=1}^{n} S_i^* A_i \Delta h_i = A \Delta b \quad (3)$$

In saturated confined aquifer-systems, skeletal storativity (S^*_k) is the main component of S^*, as it is typically greater than the amount attributed to pore-water (S_w). S^*_k sums up inputs from both coarse-grained (aquifers) and fine-grained (aquitards) sediments composing the system, with the latter being several orders of magnitude higher (Riley, 1998) and involving both elastic (recoverable) and inelastic (unrecoverable) stress ranges (S'_{ke} and S'_{kv}, respectively), as opposed to only elastic (S_{ke}) stress at aquifers (Sneed, 2001).

When hydraulic heads drop below the historical minimum experienced by the aquifer (i.e., pre-consolidation head, h_{pc}), aquitards deform inelastically, with fine-grained sediments rearrangement and pore-volume permanent reduction (Terzaghi, 1925). Thus, for compacting aquifer-systems, S'_{kv} prevails and equals (Riley, 1969):

$$S'_{\text{kv}} = S'_{\text{skv}} b_0 = \frac{\Delta b_u}{\Delta h} \quad (4)$$

where S'_{skv} is the specific storativity, b_0 the initial thickness and Δb_u the ultimate system compaction in response to a sustained Δh (Helm, 1984). Ultimate compaction is achieved when heads in the aquitard (slow-draining units, with very low hydraulic conductivity) equilibrate those in adjacent aquifers. The time for the aquifer to reach 93% Δb_u is proportional to S'_{skv} and b squared, and inversely proportional to conductivity (Riley, 1969; Scott, 1963) thus, depending on aquifer characteristics, can be months- to decades-long (Helm, 1978). On the other side, the aquitard-drainage model implies that compaction may still happen as a result of Δh, even after the heads stopped declining or started to recover.

In unconfined aquifers, groundwater is mostly released by gravity drainage rather than from specific storage, hence their storativity approximately equals the specific yield S_y (typically 0.1–0.3; Lohman, 1972).

2.3. Piezometric Monitoring

Hydraulic head change rates $\Delta h/\Delta t$ at >3,500 locations within the study area were estimated based on the national piezometric monitoring network database (CONAGUA, 2020). For each piezometer, this provides n yearly observations of the static level (l_i), going back as far as 1981, depending on instrument installation date and measurement campaigns conducted. The long-term $\Delta h/\Delta t$ was computed by linearly fitting l_i observations at each piezometer. To match the satellite observation period, the 2019–2020 $\Delta h/\Delta t$ was also calculated at 190 piezometers (where l_i data allowed).

By approximating Δb with InSAR-derived vertical displacements, the 2019–2020 $\Delta b/\Delta h$ ratio allowed a rough computation of S_y for unconfined and S'_{kv} for confined aquifers. For confined systems, this assumes Δh as representative of the average declines occurring in the coarse-grained layers during 2019–2020. When Δb_u is not yet reached, this approach enables a transient, lower-bound estimation of S'_{kv} (Figueroa-Vega et al., 1984).

2.4. Groundwater Availability

Official Mexican Standards (CONAGUA, 2015) establish that annual groundwater availability (DMA) of an aquifer-system is calculated as its total recharge minus: (a) the portion of natural discharge (D_{nc}) committed as surface water through springs and rivers, or preserved to guarantee ecosystem conservation and avoid poor quality water inflow, and (b) the total extraction volume (Q_{lic}), licensed in the Public Registry of Water Rights

(REPDA) database (CONAGUA, 2022b) or pending registration, plus reserves and regulations/planning-related volumes:

$$\mathrm{DMA} = R - D_{\mathrm{nc}} - Q_{\mathrm{lic}} \tag{5}$$

DMA indicates the groundwater amount that might be extracted from the aquifer-system, in addition to Q_{lic} and D_{nc}, without endangering the ecosystem. A status of "availability" is identified if $DMA > 0$ (or "deficit" if DMA < 0), based on which new extraction licenses can be (or cannot) be granted.

In turn, the Federal Rights Law (CONAGUA, 2021) defines the availability index (I_d) as:

$$I_d = \frac{\mathrm{DMA}}{R - D_{\mathrm{nc}}} \tag{6}$$

This allows for aquifers categorization into zones of decreasing groundwater exploitation rights cost: #1 ($I_d \leq -0.1$), #2 ($-0.1 < I_d \leq +0.1$), #3 ($+0.1 < I_d \leq +0.8$) and #4 ($I_d > +0.8$).

When DMA and/or I_d were not included in the Gazette for a specific year, they were computed according to Equations 5 and 6.

3. Results

3.1. Evolution of Groundwater Availability

Present-day DMA data show that recharge and discharge are roughly balanced for 38% of the aquifers (±5 hm^3/year), but 114 are in deficit (Figure 2a). The most notable occur at Mexico City Metropolitan Area (−507 hm^3/year) and Cuautitlán-Pachuca (−183 hm^3/year), as well as to their northwest at San Juan del Río Valley and Pénjamo-Abasolo, where extraction rates are remarkable (Figure 2b). In turn, aquifers with the lowest I_d are similarly distributed (Figure 2c), with 24% in zone #1 and negative peaks at Santa María del Río (−4.1) and Pastor Ortiz-La Piedad (−2.6), where deficits largely exceed the net natural inflows.

Multi-temporal data stacking depicts the decadal evolution recorded in 2013–2022. Only 22% aquifers show increased DMA (Figure 2d), for example, Silao-Romita (+236 hm^3/year) and León Valley (+126 hm^3/year), mainly due to decreased groundwater extraction (Figure 2e). Conversely, the greatest drops were at Los Naranjos (−166 hm^3/year) and Cuautitlán-Pachuca (−128 hm^3/year), driven by boosted extractions. The total number of overexploited systems increased from 53 in 2011 to 57 in 2022 (Figure 2f), and followed a trend similar to that characterizing the whole country. The proportion of zone #3−#4 aquifers decreased from 66% in 2014 to 54% in 2022, while zone #2 doubled and zone #1 increased by +1%.

3.2. Land Subsidence Hotspots

The InSAR survey identifies ~35.7 million coherent targets across the area (Figure 3a), with land cover-controlled distribution, hence denser networks over urbanized and arid lands (e.g., RHA VII) and sparser across rural/vegetated landscapes (e.g., coastal zones of RHAs V and X). V_U in 2019–2020 ranges within ±0.5 cm/year for most landmass, though several land subsidence hotspots are found at major cities and agricultural districts within the TMVB and, to a lesser extent, northern regions.

The main hotspots and their highest (negative) V_U in cm/year are (Figures 3b–3i): Mexico City Metropolitan Area (−45); Chaparrosa (−22), east of Fresnillo (−16), Loreto (−13), San Ramón, El Barril and San José de Lourdes (−12) in Zacatecas; Villa de Arista (−19) in San Luis Potosí; Aguascalientes Valley (−17) and city (−14); Jocotepec (−16), Ciudad Guzmán (−15) and Guadalajara (−13) in Jalisco; Tecamachalco Valley (−15) and Totolcingo (−13) in Puebla; Zamora (−12) and Morelia (−8) in Michoacán; León (−12), Irapuaro (−12), Celaya (−10) and El Saucito (−10) in Guanajuato; and Toluca (−9) in México. The survey also provides the first account of land compaction at several previously unmapped towns, including Etzlatlán and Ameca (−6) in western Jalisco, and the city of Oaxaca (−7). Subsidence at Mexico City, Aguascalientes and Morelia, its relationship with urbanization and groundwater use, and the induced risk on urban infrastructure are discussed in dedicated investigations (Cigna & Tapete, 2021a, 2021b, 2022).

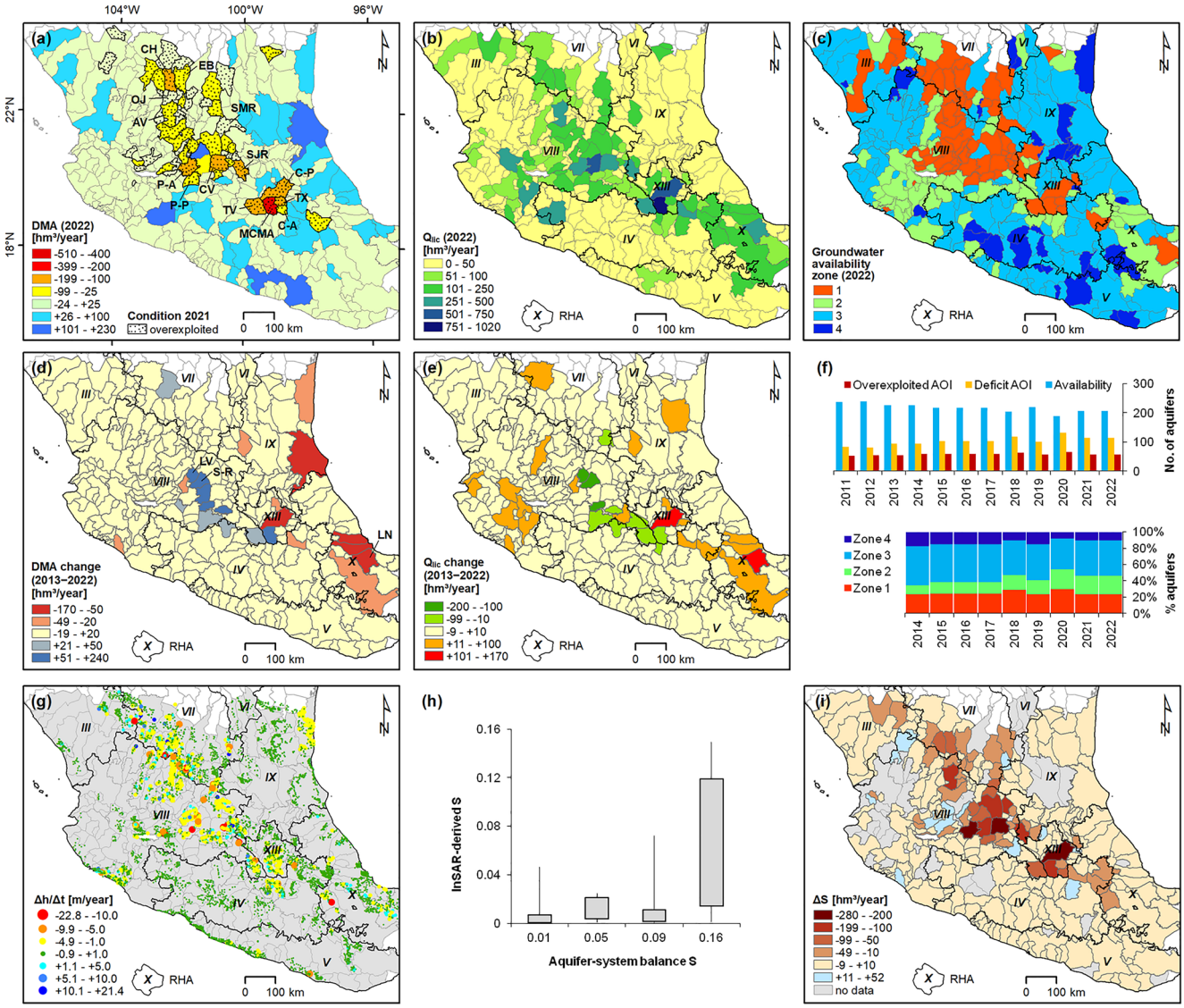

Figure 2. Groundwater availability in the aquifer-systems of Central Mexico: present-day (a) annual availability (DMA), (b) licensed extractions (Q_{lic}) and (c) zonation (CONAGUA, 2022a); changes in (d) *DMA*, (e) Q_{lic}, (f) condition and zonation; (g) long-term hydraulic head change rate ($\Delta h/\Delta t$); (h) distribution of observed storativity (S) against aquifer-system balance values (boxes: interquartile range; lines: minimum/maximum); and (i) modeled storage change (ΔS). Notation: AV, Aguascalientes Valley; C-A, Chalco-Amecameca; CH, Chupaderos; C-P, Cuautitlán-Pachuca; CV, Celaya Valley; EB, El Barril; LN, Los Naranjos; LV, León Valley; MCMA, Mexico City Metropolitan Area; OJ, Ojocaliente; P-A, Pénjamo-Abasolo; P-P, Pastor Ortiz-La Piedad; SJR, San Juan del Río Valley; SMR, Santa María del Río; S-R, Silao-Romita; TV, Toluca Valley; TX, Texcoco. Maps created with ESRI ArcMap, plots with MS Excel.

The hotspot at the southeastern margin of the area (Figure 3a) depicts the 2020 M_w 7.4 earthquake-induced deformation (Wen et al., 2021), a signal not linked with aquifer depletion, therefore filtered out in the following analysis.

3.3. Aquifer-System Storage Loss and Compaction

Hydrographs at most piezometers show steadily declining h and no obvious rises. Long-term $\Delta h/\Delta t$ exceeds −5 m/year at several sites in the TMVB and RHA VII (Figure 2g). Storativity S estimations based on InSAR and piezometric data are lower than those used for aquifer-system balance, though generally seem to correlate (Figure 2h). For systems with S_y of ∼0.05 (e.g., Calvillo Valley), estimations typically range between 0.003 and 0.021, with median at 0.008. The latter increases to 0.074 for systems with S_y of 0.16 (e.g., Aguascalientes Valley).

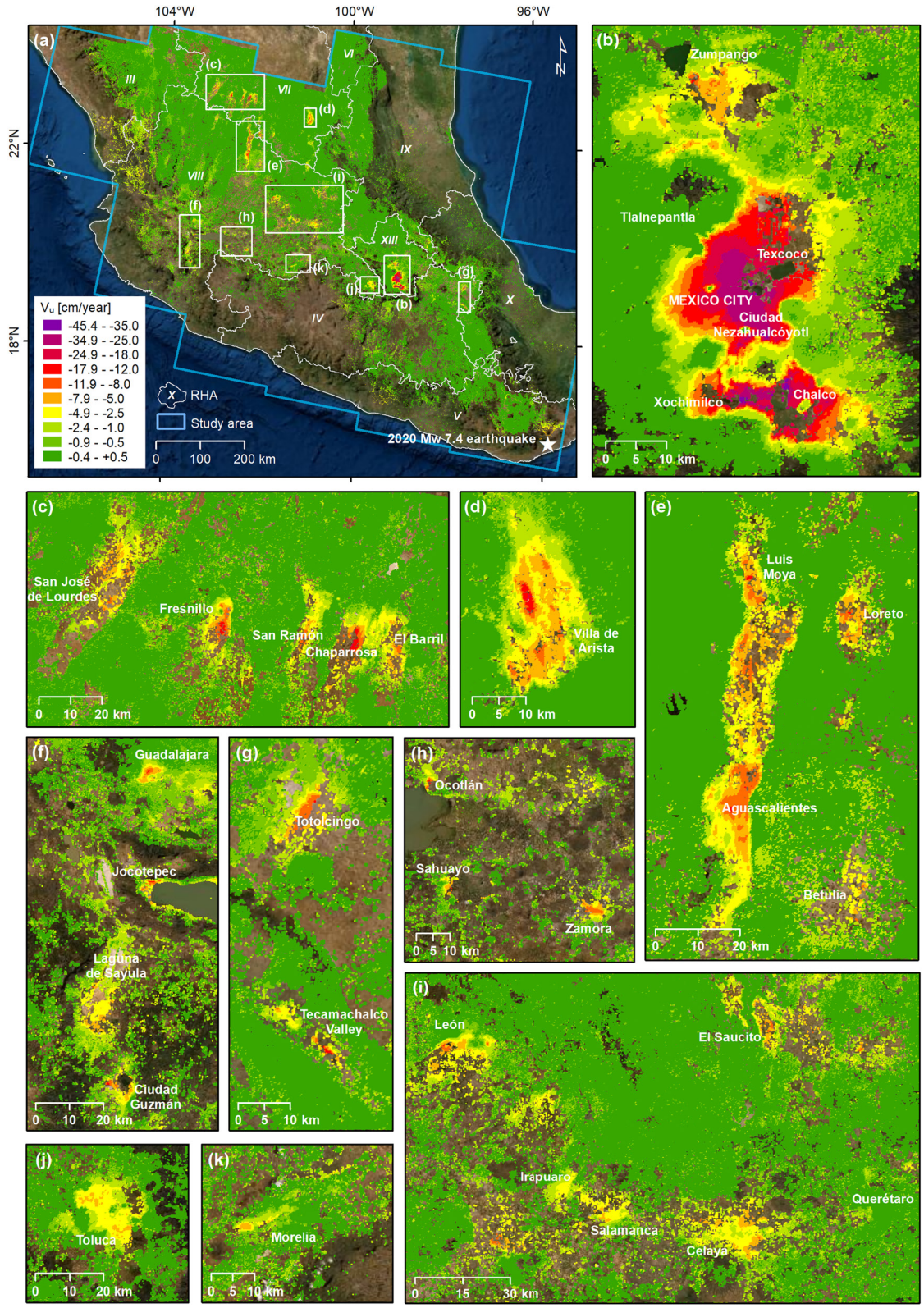
104°W
100°W
96°W
22°N
18°N
(a)
(b)
(c)
(d)
(e)
(f)
(g)
(h)
(i)
(j)
(k)
I
II
III
IV
V
VI
VII
VIII
IX
X
XIII
RHA
Study area
0 100 200 km
2020 Mw 7.4 earthquake
Vu [cm/year]
-45.4 - -35.0
-34.9 - -25.0
-24.9 - -18.0
-17.9 - -12.0
-11.9 - -8.0
-7.9 - -5.0
-4.9 - -2.5
-2.4 - -1.0
-0.9 - -0.5
-0.4 - +0.5
Zumpango
Tlalnepantla
Texcoco
MEXICO CITY
Ciudad Nezahualcóyotl
Xochimilco
Chalco
0 5 10 km
San José de Lourdes
Fresnillo
San Ramón
Chaparrosa
El Barril
0 10 20 km
Villa de Arista
0 5 10 km
Luis Moya
Loreto
Aguascalientes
Bétulia
0 10 20 km
Guadalajara
Jocotepec
Laguna de Sayula
Ciudad Guzmán
0 10 20 km
Totolcingo
Tecamachalco Valley
0 5 10 km
Ocotlán
Sahuayo
Zamora
0 5 10 km
León
El Saucito
Irapuaro
Querétaro
Salamanca
Celaya
0 15 30 km
Toluca
0 10 20 km
Morelia
0 5 10 km

Figure 3.

Highly exploited aquifer-systems loosing non-renewable storage are concentrated in RHAs VII, VIII, and XIII (Figure 2i). Here, the modeled ΔS loss rate reaches −280 (Cuautitlán-Pachuca), −215 (Pénjamo-Abasolo), and −201 (Celaya Valley) hm^3/year, resulting from withdrawal of 637, 440, and 515 hm^3/year, respectively.

InSAR-derived V_U fairly correlates with aquifer-system balance parameters (Figure 4a). Approximately 40% of the observed V_U variation across Central Mexico is explained by the variance of DMA. The figure drops to 35% and 22% when considering Q_{lic} and ΔS, respectively. The three RHAs encompassing most hotspots generally show higher correlation with each parameter, though slight different linear fits. The semi-theoretical relationships between V_U and aquifer management parameters (Figure 4a) show that, in region VII: V_U [cm/year] = $-0.08*Q_{lic}$ −1.84 (with Q_{lic} in hm^3/year); in region VIII: $V_U = -0.02*Q_{lic}$ −3.44; while in region XIII: $V_U = -0.04*Q_{lic}$ −6.61. Looking at single systems, the subsidence to licensed withdrawal rate ratio V_U/Q_{lic} is aligned with the region they belong to (e.g., in region XIII, -0.04×10^{-4} hm^{-2} at Mexico City Metropolitan Area, where Q_{lic} is 1,020 hm^3/year), or divergent due to aquifer-specific conditions (e.g., -0.16×10^{-4} hm^{-2} at Texcoco and -0.46×10^{-4} hm^{-2} at Chalco-Amecameca, where Q_{lic} is 426 and 99 hm^3/year, respectively). At Chupaderos (VII) in Zacatecas, V_U/Q_{lic} is -0.12×10^{-4} hm^{-2}.

Correlations improve for the InSAR-derived aquifer-system compaction ΔS_{sat} (Figure 4b), which appears much better explained by Q_{lic} (47%) and ΔS (30%) across the whole area. The compaction volume to withdrawal rates relationships are: ΔS_{sat} [hm^3/year] = $-0.05*Q_{lic}$ −2.09 (Central Mexico); $\Delta S_{sat} = -0.11*Q_{lic}$ −0.36 (region VII); $\Delta S_{sat} = -0.05*Q_{lic}$ −1.78 (VIII); and $\Delta S_{sat} = -0.06*Q_{lic}$ −2.75 (XIII). Single aquifer-systems often compact more than others within the RHA, for example, −0.18 $\Delta S_{sat}/Q_{lic}$ rate is observed at Chalco-Amecameca and Texcoco, three-times steeper than region XIII's. Similarly, at Ojocaliente $\Delta S_{sat}/Q_{lic}$ is −0.12, two-times steeper than region VIII's.

Across both the whole of Central Mexico and single RHAs, InSAR-derived ΔS_{sat} are ∼10%–15% of the modeled ΔS provided in the management reports.

4. Discussion

The agreement between InSAR-derived V_U and aquifer DMA confirms the association between these two variables for the whole of Central Mexico, thus spatially extending initial observations that were limited only to the Lerma-Santiago-Pacifico watershed (Castellazzi, Martel, et al., 2016). DMA is, however, a management parameter identified by CONAGUA to avoid damage to ecosystems (Section 2.4), whereas it does not (directly) quantify groundwater level/volume change in each aquifer-system. Hence, prediction of future compaction under different extraction scenarios could better be based on the aquifer-system subsidence (rate or volume) to liquid withdrawal Q_{lic} relationships, or on the site-specific subsidence to hydraulic head decline ratios $\Delta b/\Delta h$.

Despite the weak correlation between V_U and Q_{lic} observed at wells within single subsidence hotspots, such as Mexico City (Chaussard et al., 2021) and Morelia (Cigna & Tapete, 2022), our analysis provides evidence of a moderate association between compaction and extractions at aquifer-system scale (Figures 4a and 4b). Assumptions made to derive the semi-theoretical relationships (V_U to Q_{lic}, and ΔS_{sat} to Q_{lic}) are to be accounted for when exploiting them to attempt predictions. First, the relationships refer to the whole of Central Mexico or one of its RHAs, thus may not reflect the specific behavior or characteristics of a single aquifer-system (e.g., complex structure, local consolidation conditions, or aquitard thickness). For instance, city-scale investigations in Mexico City and Aguascalientes (Cigna & Tapete, 2021a, 2021b) demonstrated that the main predictor of V_U is unconsolidated sediment thickness, rather than pumping rate. Moreover, the semi-theoretical relationships do not directly account for the time-lag between head changes and aquitard compaction, or varying aquifer properties with depth and time. More sophisticated approaches at site-scale could address this (e.g., Li et al., 2022; Zhang et al., 2022). Therefore, future research may focus on testing whether the relationships could be tailored for different aquifer-system types and characteristics, by also incorporating other input variables. Lastly, estimation of ΔS_{sat} assumes that deformation is purely due to aquifer compaction. Even if long-wavelength and major unrelated

Figure 3. Land subsidence in Central Mexico detected by 2019–2020 Sentinel-1 Interferometric Synthetic Aperture Radar (InSAR): (a) regional overview and main hotspots: (b) Mexico City; (c) Chaparrosa, Fresnillo, San Ramón, El Barril and San José de Lourdes; (d) Villa de Arista; (e) Loreto and Aguascalientes Valley; (f) Jocotepec, Ciudad Guzmán and Guadalajara; (g) Tecamachalco Valley and Totolcingo; (h) Zamora, Sahuayo and Ocotlán; (i) León, Irapuaro, Salamanca, Celaya and El Saucito; (j) Toluca; and (k) Morelia. Maps created with ESRI ArcMap. Basemap credits: ESRI, DigitalGlobe, GeoEye, Earthstar Geographics, CNES/Airbus DS, USDA, USGS, AeroGRID, IGN, and GIS User Community.

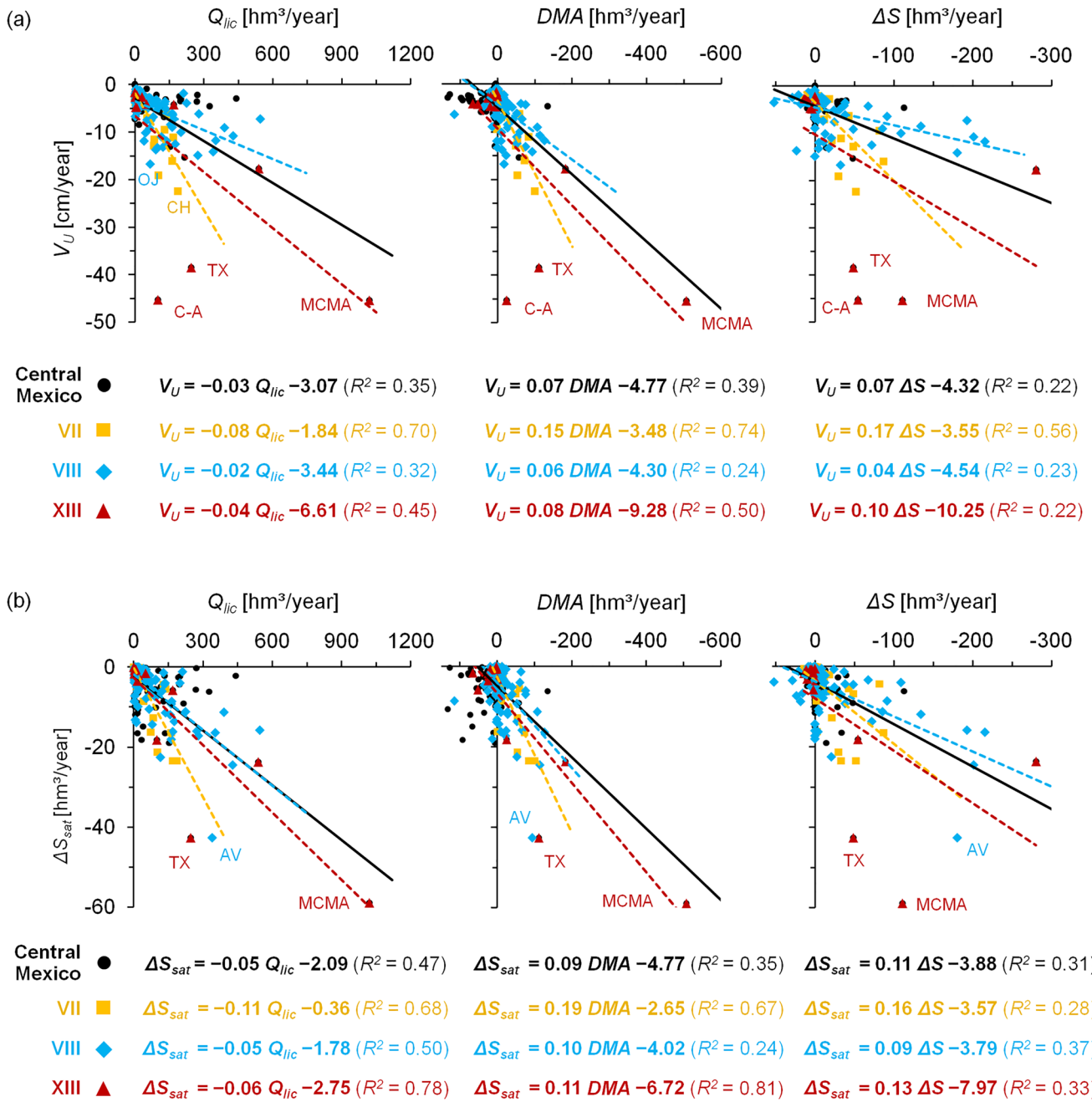

Figure 4. Correlation between land subsidence and aquifer-system balance parameters in Central Mexico. Licensed groundwater withdrawal (Q_{lic}), annual groundwater availability (DMA) and modeled storage change (ΔS) are compared with Interferometric Synthetic Aperture Radar (InSAR)-derived (a) highest (negative) vertical displacement velocity (V_U) and (b) total compaction volume rate (ΔS_{sat}) at each aquifer-system. Linear fits with determination coefficients (R^2) are provided for the whole area (solid black line) and regions VII, VIII, and XIII (dashed lines). Notation: AV, Aguascalientes Valley; C-A, Chalco-Amecameca; CH, Chupaderos; MCMA, Mexico City Metropolitan Area; OJ, Ojocaliente; TX, Texcoco. Plots created with MS-Excel.

signals were masked out (Section 2.1), any local scale process (e.g., settlement due to engineering works) might still contribute to ΔS_{sat}, though only marginally, compared with aquifer compaction signals.

For normally consolidated systems, the steadily declining Δh at the piezometers of the national network suggests that, at those sites, heads increasingly dropped below h_{pc}, thus exceeding pre-consolidation stress and causing irreversible aquifer-system deformation. InSAR-derived S and compaction therefore reflect inelastic components only, and $\Delta b/\Delta h$ relationships provide a lower limit of subsidence magnitude in response to further step-increase

in effective stress beyond the pre-consolidation value (Figueroa-Vega et al., 1984). Anyway, the yearly temporal granularity of the piezometric data prevents the detection of short-term or seasonal signals, therefore any short-term variations cannot be investigated with the available dataset.

Subsidence and Δh generally show low correlation within single hotspots, for example, Mexico City (Solano Rojas et al., 2015), Aguascalientes (Cigna & Tapete, 2021b) and Morelia (Cigna et al., 2012), given the leading role of other factors in determining compaction rates and patterns (e.g., aquitard thickness, geological structures). Nevertheless, the moderate agreement between the storativity S used for aquifer-system modeling and InSAR-derived values at the monitoring network (Figure 2h) encourages future research efforts to investigate the relationship between Δh and compaction across the region. Discerning storativity components for unconfined and confined layers of the same system would also require further investigation. The discrepancies between observed compaction volumes and modeled storage changes (ΔS_{sat} vs. ΔS) could part be explained by the different time periods, namely, 2019–2020 for the InSAR survey versus as far as the 1980s for the reference aquifer-system studies. In some cases, indeed, the higher modeled ΔS figures could be driven by greater extraction rates adopted in the past. Another potential influence may come from assumptions made during the modeling (e.g., use of a single-layer system, with homogeneous S throughout), which could mask out site-specific conditions. The transient nature of S estimations until ultimate compaction (Sections 2.2−2.3) could also play a role in lowering down InSAR-derived figures.

5. Conclusions

There is general consensus that in several areas of Central Mexico groundwater is extracted at the expense of non-renewable storage of aquifer-systems, causing land subsidence and other environmental impacts (e.g., saltwater intrusion, quality degradation, spring discharge and river flow reduction). This work provides semi-theoretical relationships (Figure 4) to link groundwater use information at aquifer-system scale with compaction and storage loss, potentially enabling predictions of subsidence rates and volumes for different groundwater management scenarios. While these relationships may need further tailoring at local scale, they provide a first high-level assessment of the potential additional compaction resulting from increased pressure on groundwater resources (or also, reduced pressure induced by managed recharge; Cruz-Ayala & Megdal, 2020). Given population growth and renewable freshwater availability drop expected in 2030 (CONAGUA, 2022b), this is key information to feed into decision making and water management strategies.

Data Availability Statement

Aquifer management data are freely distributed by CONAGUA (https://sigagis.conagua.gob.mx/gas1/sections/Disponibilidad_Acuiferos.html), while Sentinel-1 and Sentinel-2 imagery by ESA via Copernicus Open Access Hub, after user registration and catalog search (https://scihub.copernicus.eu/).

Acknowledgments
Sentinel-1 data processing in GEP was supported by ESA Network of Resources Initiative (project id. 190791). Terradue S.r.l. is acknowledged for providing technical support with the GEP platform, and CNR-IREA for making P-SBAS available. Open Access Funding provided by Consiglio Nazionale delle Ricerche within the CRUI-CARE Agreement.

References

Bell, J. W., Amelung, F., Ferretti, A., Bianchi, M., & Novali, F. (2008). Permanent scatterer InSAR reveals seasonal and long-term aquifer-system response to groundwater pumping and artificial recharge. *Water Resources Research*, *44*(2). https://doi.org/10.1029/2007WR006152

Blewitt, G., Hammond, W., & Kreemer, C. (2018). Harnessing the GPS data explosion for interdisciplinary science. *Eos*, *99*. https://doi.org/10.1029/2018eo104623

Bonì, R., Cigna, F., Bricker, S., Meisina, C., & McCormack, H. (2016). Characterisation of hydraulic head changes and aquifer properties in the London Basin using persistent scatterer interferometry ground motion data. *Journal of Hydrology*, *540*, 835–849. https://doi.org/10.1016/j.jhydrol.2016.06.068

Brunori, C. A., Bignami, C., Albano, M., Zucca, F., Samsonov, S., Groppelli, G., et al. (2015). Land subsidence, ground fissures and buried faults: InSAR monitoring of Ciudad Guzmán (Jalisco, Mexico). *Remote Sensing*, *7*(7), 8610–8630. https://doi.org/10.3390/rs70708610

Cabral-Cano, E., Dixon, T. H., Miralles-Wilhelm, F., Díaz-Molina, O., Sánchez-Zamora, O., & Carande, R. E. (2008). Space geodetic imaging of rapid ground subsidence in Mexico City. *Bulletin of the Geological Society of America*, *120*(11–12), 1556–1566. https://doi.org/10.1130/B26001.1

Carreón Freyre, D. (2010). (Vol. 339, pp. 149–157). Land subsidence processes and associated ground fracturing in Central Mexico. *Proceedings of EISOLS 2010, Land Subsidence, Associated Hazards and the Role of Natural Resources Development*.Red Book Series Publication.

Carreon-Freyre, D., Cerca, M., Ochoa González, G. H., Ortiz-Villaseñor, I., Gámez-González, J., & Gutiérrez-Calderón, R. (2011). Land subsidence and ground fracturing affecting major cities of central Mexico and related groundwater management. In *Proceedings of 14th pan-American conference on soil mechanics and geotechnical engineering - 64th Canadian geotechnical conference* (pp. 2–6). Retrieved from https://www.issmge.org/publications/publication/land-subsidence-and-ground-fracturing-affecting-major-cities-of-central-mexico-and-related-groundwater-management

Castellazzi, P., Arroyo-Domínguez, N., Martel, R., Calderhead, A. I., Normand, J. C. L., Gárfias, J., & Rivera, A. (2016). Land subsidence in major cities of Central Mexico: Interpreting InSAR-derived land subsidence mapping with hydrogeological data. *International Journal of Applied Earth Observation and Geoinformation*, *47*, 102–111. https://doi.org/10.1016/j.jag.2015.12.002

Castellazzi, P., Longuevergne, L., Martel, R., Rivera, A., Brouard, C., & Chaussard, E. (2018). Quantitative mapping of groundwater depletion at the water management scale using a combined GRACE/InSAR approach. *Remote Sensing of Environment*, *205*, 408–418. https://doi.org/10.1016/j.rse.2017.11.025

Castellazzi, P., Martel, R., Rivera, A., Huang, J., Pavlic, G., Calderhead, A. I., et al. (2016). Groundwater depletion in Central Mexico: Use of GRACE and InSAR to support water resources management. *Water Resources Research*, *52*(8), 5985–6003. https://doi.org/10.1002/2015WR018211

Casu, F., Elefante, S., Imperatore, P., Zinno, I., Manunta, M., De Luca, C., & Lanari, R. (2014). SBAS-DInSAR parallel processing for deformation time-series computation. *IEEE Journal of Selected Topics in Applied Earth Observations and Remote Sensing*, *7*(8), 3285–3296. https://doi.org/10.1109/JSTARS.2014.2322671

Chaussard, E., Bürgmann, R., Shirzaei, M., Fielding, E. J., & Baker, B. (2014). Predictability of hydraulic head changes and characterization of aquifer-system and fault properties from InSAR-derived ground deformation. *Journal of Geophysical Research: Solid Earth*, *119*(8), 6572–6590. https://doi.org/10.1002/2014JB011266

Chaussard, E., Havazli, E., Fattahi, H., Cabral-Cano, E., & Solano-Rojas, D. (2021). Over a century of sinking in Mexico City: No hope for significant elevation and storage capacity recovery. *Journal of Geophysical Research: Solid Earth*, *126*(4), e2020JB020648. https://doi.org/10.1029/2020JB020648

Chaussard, E., Wdowinski, S., Cabral-Cano, E., & Amelung, F. (2014). Land subsidence in central Mexico detected by ALOS InSAR time-series. *Remote Sensing of Environment*, *140*, 94–106. https://doi.org/10.1016/j.rse.2013.08.038

Cigna, F., Esquivel Ramírez, R., & Tapete, D. (2021). Accuracy of Sentinel-1 PSI and SBAS InSAR displacement velocities against GNSS and geodetic leveling monitoring data. *Remote Sensing*, *13*(23), 4800. https://doi.org/10.3390/rs13234800

Cigna, F., Osmanoğlu, B., Cabral-Cano, E., Dixon, T. H., Ávila-Olivera, J. A., Garduño-Monroy, V. H., et al. (2012). Monitoring land subsidence and its induced geological hazard with Synthetic Aperture Radar Interferometry: A case study in Morelia, Mexico. *Remote Sensing of Environment*, *117*, 146–161. https://doi.org/10.1016/j.rse.2011.09.005

Cigna, F., & Tapete, D. (2021a). Present-day land subsidence rates, surface faulting hazard and risk in Mexico City with 2014–2020 Sentinel-1 IW InSAR. *Remote Sensing of Environment*, *253*, 1–19. https://doi.org/10.1016/j.rse.2020.112161

Cigna, F., & Tapete, D. (2021b). Satellite InSAR survey of structurally-controlled land subsidence due to groundwater exploitation in the Aguascalientes Valley, Mexico. *Remote Sensing of Environment*, *254*, 1–23. https://doi.org/10.1016/j.rse.2020.112254

Cigna, F., & Tapete, D. (2022). Urban growth and land subsidence: Multi-decadal investigation using human settlement data and satellite InSAR in Morelia, Mexico. *Science of the Total Environment*, *811*, 152211. https://doi.org/10.1016/j.scitotenv.2021.152211

Cigna, F., Tapete, D., Garduño-Monroy, V. H. V. H., Muñiz-Jauregui, J. A. J. A., García-Hernández, O. H. O. H., & Jiménez-Haro, A. (2019). Wide-area InSAR survey of surface deformation in urban areas and geothermal fields in the eastern Trans-Mexican Volcanic Belt, Mexico. *Remote Sensing*, *11*(20), 2341. https://doi.org/10.3390/rs11202341

CONAGUA. (2015). Norma Oficial Mexicana NOM-011-CONAGUA-2015, Conservación del recurso agua-Que establece las especificaciones y el método para determinar la disponibilidad media anual de las aguas nacionales. Retrieved from https://www.dof.gob.mx/nota_detalle.php?codigo=5387027%26fecha=27/03/2015

CONAGUA. (2020). Red piezométrica Mapas. [Data Set]. (Version 24/07/2020). Retrieved January 19, 2022, from https://datos.gob.mx/busca/dataset/red-piezometrica-mapas

CONAGUA. (2021). Ley Federal de Derechos. Disposiciones Aplicables en Materia de Aguas Nacionales 2021. Retrieved from https://www.gob.mx/cms/uploads/attachment/file/635527/CGRF-1-21_LFD_VF.pdf

CONAGUA. (2022a). Aguas subterráneas. Retrieved January 18, 2022, from https://sigagis.conagua.gob.mx/gas1/index.html

CONAGUA. (2022b). Sistema Nacional de Información del Agua. Retrieved from http://sina.conagua.gob.mx/sina/index.php

Cruz-Ayala, M. B., & Megdal, S. B. (2020). An overview of managed aquifer recharge in Mexico and its legal framework. *Water (Switzerland)*, *12*(2), 474. https://doi.org/10.3390/w12020474

Farr, T. G., Rosen, P. A., Caro, E., Crippen, R., Duren, R., Hensley, S., et al. (2007). The shuttle radar topography mission. *Reviews of Geophysics*, *45*(2), RG2004. https://doi.org/10.1029/2005RG000183

Ferrari, L., Orozco-Esquivel, T., Manea, V., & Manea, M. (2012). The dynamic history of the Trans-Mexican Volcanic Belt and the Mexico subduction zone. *Tectonophysics*, *522–523*, 122–149. https://doi.org/10.1016/j.tecto.2011.09.018

Figueroa-Miranda, S., Tuxpan-Vargas, J., Ramos-Leal, J. A., Hernández-Madrigal, V. M., & Villaseñor-Reyes, C. I. (2018). Land subsidence by groundwater over-exploitation from aquifers in tectonic valleys of central Mexico: A review. *Engineering Geology*, *246*, 91–106. https://doi.org/10.1016/j.enggeo.2018.09.023

Figueroa-Vega, G., Yamamoto, S., & Group, W. (1984). Techniques for prediction of subsidence. In J. F. Poland (Ed.), *Guidebook to studies of land subsidence due to ground-water withdrawal* (pp. 89–117).

Galloway, D. L., & Burbey, T. J. (2011). Review: Regional land subsidence accompanying groundwater extraction. *Hydrogeology Journal*, *19*(8), 1459–1486. https://doi.org/10.1007/s10040-011-0775-5

Gleeson, T., Wada, Y., Bierkens, M. F. P., & Van Beek, L. P. H. (2012). Water balance of global aquifers revealed by groundwater footprint. *Nature*, *488*(7410), 197–200. https://doi.org/10.1038/nature11295

Helm, D. C. (1978). Field verification of a one-dimensional mathematical model for transient compaction and expansion of a confined aquifer system. In *American society of civil engineers*. In *Verification of mathematical and physical models in hydraulic engineering: Proceedings, 26th annual Hydraulics Division specialty conference* (Vol. August 9–11, pp. 189–196). University of Maryland, College Park, Maryland.

Helm, D. C. (1984). Field-based computational techniques for predicting subsidence due to fluid withdrawal. *GSA Reviews in Engineering Geology*, (Vol. 6, pp. 1–22). Geological Society of America. https://doi.org/10.1130/REG6-p1

Hernandez, A. (2003). Water law in the republic of Mexico. *United States-Mexico Law Journal*, *11*. https://doi.org/10.25922/0zrx-xr72

Hoffmann, J., Zebker, H. A., Galloway, D. L., & Amelung, F. (2001). Seasonal subsidence and rebound in Las Vegas Valley, Nevada, observed by Synthetic Aperture Radar Interferometry. *Water Resources Research*, *37*(6), 1551–1566. https://doi.org/10.1029/2000WR900404

INEGI. (2022). Censo Población y Vivienda. Retrieved from https://www.inegi.org.mx/programas/ccpv

Kachadourian-Marras, A., Alconada-Magliano, M. M., Carrillo-Rivera, J. J., Mendoza, E., Herrerías-Azcue, F., & Silva, R. (2020). Characterization of surface evidence of groundwater flow systems in continental Mexico. *Water*, *12*(9), 2459. https://doi.org/10.3390/w12092459

Li, J., Zhu, L., Gong, H., Zhou, J., Dai, Z., Li, X., et al. (2022). Unraveling elastic and inelastic storage of aquifer systems by integrating fast independent component analysis and a variable preconsolidation head decomposition method. *Journal of Hydrology*, *606*, 127420. https://doi.org/10.1016/j.jhydrol.2021.127420

Lohman, S. W. (1972). *Ground-water hydraulics*. U.S. Geological Survey Prof. Paper 708. https://doi.org/10.3133/pp708

Manunta, M., De Luca, C., Zinno, I., Casu, F., Manzo, M., Bonano, M., et al. (2019). The parallel SBAS approach for Sentinel-1 interferometric wide swath deformation time-series generation: Algorithm description and products quality assessment. *IEEE Transactions on Geoscience and Remote Sensing*, *57*(9), 6259–6281. https://doi.org/10.1109/TGRS.2019.2904912

Miller, M. M., Shirzaei, M., & Argus, D. (2017). Aquifer Mechanical properties and decelerated compaction in Tucson, Arizona. *Journal of Geophysical Research: Solid Earth*, *122*(10), 8402–8416. https://doi.org/10.1002/2017JB014531

Ojha, C., Shirzaei, M., Werth, S., Argus, D. F., & Farr, T. G. (2018). Sustained groundwater loss in California's Central Valley exacerbated by intense drought periods. *Water Resources Research*, *54*(7), 4449–4460. https://doi.org/10.1029/2017WR022250

Osmanoğlu, B., Dixon, T. H., Wdowinski, S., Cabral-Cano, E., & Jiang, Y. (2011). Mexico City subsidence observed with persistent scatterer InSAR. *International Journal of Applied Earth Observation and Geoinformation*, *13*(1), 1–12. https://doi.org/10.1016/j.jag.2010.05.009

Pacheco-Martínez, J., Cabral-Cano, E., Wdowinski, S., Hernández-Marín, M., Ortiz-Lozano, J., & Zermeño-de-León, M. (2015). Application of InSAR and Gravimetry for Land Subsidence Hazard Zoning in Aguascalientes, Mexico. *Remote Sensing*, *7*(12), 17035–17050. https://doi.org/10.3390/rs71215868

Poland, J. F., Lofgren, B. E., & Riley, F. S. (1972). Glossary of selected terms useful in studies of the mechanics of aquifer systems and land subsidence due to fluid withdrawal. *Geological Survey Water-Supply*. Paper 2025. https://doi.org/10.3133/wsp2025

Riley, F. S. (1969). Analysis of borehole extensometer data from central California. *Land Subsidence*, *2*, 423–431.

Riley, F. S. (1998). Mechanics of aquifer systems—The scientific legacy of Joseph F. Poland. In J. W. Borchers (Ed.), *Landsubsidence case studies and current research: Proceedings of the Dr. Joseph F. Poland Symposium on LandSubsidence*. *Association of Engineering Geologists Special Publication* (Vol. 8, pp. 13–27). Star Publishing Co.

Rosen, P. A., Hensley, S., Joughin, I. R., Li, F. K., Madsen, S. N., Rodriguez, E., & Goldstein, R. M. (2000). Synthetic aperture radar interferometry. *Proceedings of the IEEE*, *88*(3), 333–380. https://doi.org/10.1109/5.838084

Scott, R. F. (1963). *Principles of soil mechanics*. Addison-Wesley Pub. Co. Retrieved from https://www.worldcat.org/title/principles-of-soil-mechanics/oclc/561751

Secretaríade Gobernación. (2021a). ACUERDO por el que se dan a conocer las zonas de disponibilidad que corresponden a las cuencas y acuíferos del país para el ejerciciofiscal 2021, en términos del último párrafo del artículo 231 de la Ley Federal de Derechos vigente. Retrieved from http://www.dof.gob.mx/nota_detalle.php?codigo=5614593%26fecha=26/03/2021

Secretaríade Gobernación. (2021b). ACUERDO por el que se dan a conocer los valores de cada una de las variables que integran las fórmulas para determinar durante el ejercicio fiscal 2021 las zonas de disponibilidad […]. Retrieved from https://dof.gob.mx/2021/SEMARNAT/SEMARNAT_260221.pdf

Shiklomanov, I. A. (1993). World fresh water resources. In P. H. Gleick (Ed.), *Water in crisis: A guide to the world's fresh water resources* (pp. 13–24). Oxford University Press.

Sneed, M. (2001). Hydraulic and mechanical properties affecting ground-water flow and aquifer-system compaction, San Joaquin Valley, California. Open-File Report 01-35. https://doi.org/10.3133/OFR0135

Solano Rojas, D., Cabral Cano, E., Hernández Espriú, A., Wdowinski, S., DeMets, C., Salazar Tlaczani, L., et al. (2015). La relación de subsidencia del terreno InSAR-GPS y el abatimiento del nivel estático en pozos de la zona Metropolitana de la Ciudad de México. *Boletín de La Sociedad Geológica Mexicana*, *67*(2), 273–283. https://doi.org/10.18268/bsgm2015v67n2a10

Terzaghi, K. (1925). Settlement and consolidation of clay. *Principles of soil mechanics*, (Vol. 95, pp. 874–878). McGraw-Hill.

Torres, R., Snoeij, P., Geudtner, D., Bibby, D., Davidson, M., Attema, E., et al. (2012). GMES Sentinel-1 mission. *Remote Sensing of Environment*, *120*, 9–24. https://doi.org/10.1016/j.rse.2011.05.028

United Nations. (2022). *The United Nations world water development report 2022: Groundwater: Making the invisible visible*. UNESCO (ISBN: 978-92-3-100507-7).

Wada, Y., Van Beek, L. P. H., Van Kempen, C. M., Reckman, J. W. T. M., Vasak, S., & Bierkens, M. F. P. (2010). Global depletion of groundwater resources. *Geophysical Research Letters*, *37*(20). https://doi.org/10.1029/2010GL044571

Wen, Y., Xiao, Z., He, P., Zang, J., Liu, Y., & Xu, C. (2021). Source characteristics of the 2020 Mw 7.4 Oaxaca, Mexico, earthquake estimated from GPS, InSAR, and Teleseismic waveforms. *Seismological Research Letters*, *92*(3), 1900–1912. https://doi.org/10.1785/0220200313

Zhang, X., Chen, B., Gong, H., Lei, K., Zhou, C., Lu, Z., & Zhao, D. (2022). Inversion of groundwater storage variations considering lag effect in Beijing Plain, from RadarSat-2 with SBAS-InSAR Technology. *Remote Sensing*, *14*(4), 991. https://doi.org/10.3390/rs14040991